A Three-Dimensional Variational Data Assimilation System for MM5: Implementation and Initial Results

D. M. BARKER, W. HUANG, Y.-R. GUO, A. J. BOURGEOIS, AND Q. N. XIAO

National Center for Atmospheric Research, Boulder, Colorado

(Manuscript received 3 February 2003, in final form 13 October 2003)

ABSTRACT

A limited-area three-dimensional variational data assimilation (3DVAR) system applicable to both synoptic and mesoscale numerical weather prediction is described. The system is designed for use in time-critical real-time applications and is freely available to the data assimilation community for general research.

The unique features of this implementation of 3DVAR include (a) an analysis space represented by recursive filters and truncated eigenmodes of the background error covariance matrix, (b) the inclusion of a cyclostrophic term in 3DVAR's explicit mass–wind balance equation, and (c) the use of the software architecture of the Weather Research and Forecast (WRF) model to permit efficient performance on distributed-memory platforms.

The 3DVAR system is applied to a multiresolution, nested-domain forecast system. Resolution and seasonal-dependent background error statistics are presented. A typhoon bogusing case study is performed to illustrate the 3DVAR response to a single surface pressure observation and its subsequent impact on numerical forecasts of the fifth-generation Pennsylvania State University–National Center for Atmospheric Research Mesoscale Model (MM5). Results are also presented from an initial real-time MM5-based application of 3DVAR.

1. Introduction

Modern numerical weather prediction (NWP) data assimilation systems use information from a range of sources in order to provide a best estimate of the atmospheric state—the analysis—at a given time. Estimates of atmospheric variables from (incomplete and imperfect) observation systems may be supplemented with information from previous forecasts (the so-called background or first guess), detailed error statistics, and the laws of physics.

In recent years much effort has been spent in the development of variational data assimilation systems to replace previously used schemes, for example, optimum interpolation (Parrish and Derber 1992; Rabier et al. 2000; Lorenc et al. 2000). Advantages of the variational approach include (a) the ability to assimilate observed quantities related nontrivially to standard atmospheric variables (e.g., radiances) and (b) the imposition of dynamic balance either implicitly through the inclusion of the forecast model itself [four-dimensional variational data assimilation (4DVAR)] or explicitly through the use of balance equations (3DVAR).

This paper describes initial results from the three-dimensional variational data assimilation (3DVAR) system designed and built for the nonhydrostatic fifth-generation Pennsylvania State University–National Center for Atmospheric Research Mesoscale Model (MM5) modeling system (Dudhia 1993). The MM5 model uses a sigma-type vertical coordinate based on reference pressure and an ''Arakawa-B'' grid stagger. MM5 equations are fully compressible and are implemented numerically using a leapfrog time step and the split-explicit time scheme of Klemp and Wilhelmson (1978).

The initial goals in the development of 3DVAR for MM5 include the following.

- Release as a research community data assimilation system.
- Implementation in the Advanced Operational Aviation Weather System (AOAWS) of the Taiwan Civil Aeronautics Administration (CAA).
- Replacement of the multivariate optimum interpolation (MVOI) system in the operational, multitheater MM5-based system run by the U.S. Air Force Weather Agency (AFWA) at Offutt Air Force Base in Omaha, Nebraska.

AFWA 3DVAR implementation results will be described in a future paper. Here, results from 3DVAR within the triple, two-way nested (135/45/15 km resolution) MM5 domains (Fig. 1) of the AOAWS are described.

In addition to the earlier MM5-based motivations, the MM5 3DVAR system has been adopted as the starting point for a data assimilation capability for the Weather Research and Forecasting (WRF) model (Michalakes et

Corresponding author address: Dr. Dale Barker, NCAR/MMM, P.O. Box 3000, Boulder, CO 80307-3000.
E-mail: dmbarker@ucar.edu

al. 2001). The WRF model is a multiagency, collaborative effort to build a convective–mesoscale (1–10-km resolution range) model for use by both research and operational communities. Current major WRF partners include NCAR, the National Oceanic and Atmospheric Administration's (NOAA)'s National Center for Environmental Prediction (NCEP), NOAA Forecast Systems Laboratory (FSL), AFWA, and the Center for the Analysis and Prediction of Storms (CAPS) at Oklahoma University. The decision to use MM5 3DVAR as a starting point for WRF data assimilation was made by the WRF 3DVAR working group (WG4) following an initial assessment of the various 3DVAR codes available. The choice is based on (i) clarity (e.g., inline documentation, use of FORTRAN90-derived data types), (ii) portability to a wide variety of computing systems, and (iii) flexibility to, for example, new observation types and choice of analysis variables of the MM5 3DVAR system.

In order to focus limited resources on a single data assimilation system, and to provide a relatively seamless transition for MM5 data assimilation researchers to WRF in the future, the 3DVAR system runs in either the MM5 or WRF environments, the choice being made through name list options at run time.

Although the MM5 3DVAR code is new, the particular 3DVAR implementation discussed here is similar in basic design to that implemented operationally at the UK Meteorological Office (Lorenc et al. 2000). Further details of unique aspects of the MM5 3DVAR system are presented in the following sections. A more complete technical description of the MM5 3DVAR algorithm is contained in Barker et al. (2003). In summary, the main features are as follows.

- Incremental formulation of the model-space cost function (Courtier et al. 1994); observations are assimilated to provide analysis *increments*, which may be computed at lower resolution than the first guess forecast to reduce computational expense. Also, analysis imbalance is kept to a minimum as the first guess forecast, to which (typically small) increments are added to produce the analysis, is already a balanced, short-range forecast of the nonlinear model.
- Quasi-Newton minimization (Liu and Nocedal 1989). Convergence is defined as a specified reduction in the norm of the cost function gradient (e.g., 1% of initial value).
- Analysis increments computed on an unstaggered ''Arakawa-A'' grid. In the MM5/WRF environments, the input background wind field is interpolated from the Arakawa-B/C grid. Following minimization, the unstaggered wind analysis increments are interpolated to the B/C-grid of MM5/WRF, combined with the background field and output. Initially, 3DVAR's grid was the B-grid of MM5. This was changed to the A-grid as part of the agreement to use the code as the starting point for WRF 3DVAR. Tests indicate only minor impacts of this change on the structure of analysis increments.
- Analysis vertical levels are those of the input background forecast. The 3DVAR system is flexible to either height-based (MM5) or mass-based (WRF) vertical coordinates.
- Preconditioning of the background cost function is via a ''control variable transform'' $\mathbf{U}$ defined as $\mathbf{B} = \mathbf{U}\mathbf{U}^{\mathrm{T}}$ where $\mathbf{B}$ is the background error covariance matrix (see later).
- Control variables include streamfunction, velocity potential, ''unbalanced'' pressure, and a humidity variable (specific or relative humidity).
- Balance between mass and wind increments is achieved via a geostrophically and cyclostrophically balanced pressure derived from the wind increments. A statistical regression is used to ensure the balance is used only where it is appropriate (e.g., the balanced pressure increments are filtered in the Tropics). The formulation permits the future inclusion of additional terms, for example, frictional effects.
- ''Climatological'' background error covariances and statistical regression coefficients are estimated via the National Meteorological Center (NMC) method of averaged forecast differences (Parrish and Derber 1992). Sequences (e.g., 1 month) of MM5 forecast differences are converted to control variables space, from which an averaged (in time and longitude) vertical component of background error covariance is calculated. This matrix is then decomposed into eigenvectors/values of each control variable. Background error length scales are estimated for each vertical mode of each control variable. Background error variances/length scales are finally tuned using observation-based estimates of background/observation error.
- Representation of the horizontal component of background error is via horizontally isotropic and homogeneous recursive filters. The vertical component is applied through projection onto climatologically averaged (in time, longitude, and optionally latitude) eigenvectors of vertical error estimated via the NMC-method. Horizontal/vertical errors are nonseparable in that horizontal scales vary with vertical eigenvectors.
- Parallelization uses the software architecture of WRF (Michalakes et al. 2001).

Atmospheric observations are both incomplete and imperfect. The optimal use of observations and prior (e.g., background) information therefore depends crucially on the accuracy of observation and background errors. Also, approximations to dynamical and physical processes are frequently required in practical implementations of variational data assimilation algorithms. The accuracy of the assimilation is therefore reduced in areas where these approximations are inaccurate.

Given the preexistence of an MM5 4DVAR capability (Zou et al. 1997), it is perhaps necessary to discuss the reasons for developing a new 3DVAR system for use

with the MM5. The major goal for the project has been to design a single VAR system suitable for operational implementation in CAA AOAWS and AFWA environments. The computation resources required to run MM5 4DVAR are well beyond the available resources of these applications. Also, a well-designed 3DVAR system provides a sound base from which to upgrade to a 4DVAR capability (e.g., 4DVAR for WRF for which the 3DVAR system described here is also being developed). Many of the algorithms required by 4DVAR (observation operators, minimization packages, preconditioning methods, balance constraints, background error covariances, data assimilation diagnostics, etc.) are contained within 3DVAR, which therefore provides an environment for researchers to investigate these crucial aspects of the data assimilation system. The only significant omission required for 4DVAR is a forecast adjoint model and, in the case of incremental 4DVAR, the corresponding linear model used to describe the evolution of finite perturbations.

Increases in available computing power now permit the operational implementation of 4DVAR (Rabier et al. 2000) and other more computationally intensive techniques, for example, Kalman filters (Houtekamer and Mitchell 1998; Anderson 2001). However, alternative uses of increased computing power exist, for example, ensemble forecast systems or the assimilation of additional high-density (underused and expensive) observations. The best use of resources will be application dependent, but it is probable that 3DVAR will continue to be a valuable data assimilation tool for research and training of those new to the field of data assimilation for the foreseeable future.

The remainder of this paper is laid out as follows. In section 2, further details of the 3DVAR implementation are given. Section 3 presents a case study that assesses the impact of a single surface pressure observation on the 3DVAR analysis and subsequent forecast evolution of a hurricane. Example forecast verification from the AOAWS implementation of 3DVAR is given in section 4. Conclusions are presented in section 5 together with a summary of plans to extend the capabilities of the community 3DVAR system.

2. Practical implementation of 3DVAR

In general terms, VAR systems may be categorized as those data assimilation systems which provide an analysis $\mathbf{x}^a$ via the minimization of a prescribed cost function $J(\mathbf{x})$, (e.g., Ide et al. 1997)

$$\begin{aligned} J(\mathbf{x}) &= J^b + J^o \\ &= \frac{1}{2}(\mathbf{x} - \mathbf{x}^b)^{\mathrm{T}}\mathbf{B}^{-1}(\mathbf{x} - \mathbf{x}^b) \\ &\quad + \frac{1}{2}(\mathbf{y} - \mathbf{y}^o)^{\mathrm{T}}(\mathbf{E} + \mathbf{F})^{-1}(\mathbf{y} - \mathbf{y}^o). \end{aligned} \quad (1)$$

In (1), the analysis $\mathbf{x} = \mathbf{x}^a$ represents the a posteriori maximum likelihood (minimum variance) estimate of the true state of the atmosphere given two sources of data: the background (previous forecast) $\mathbf{x}^b$ and observations $\mathbf{y}^o$ (Lorenc 1986). The analysis fit to this data is weighted by estimates of their errors: $\mathbf{B}$, $\mathbf{E}$, and $\mathbf{F}$ are the background, observation (instrumental), and representiveness error covariance matrices, respectively. Representiveness error is an estimate of inaccuracies introduced in the observation operator H used to transform the gridpoint analysis $\mathbf{x}$ to observation space $\mathbf{y} = H(\mathbf{x})$. This error will be resolution dependent and may also include a contribution from approximations in H.

The cost function (1) assumes that observation and background error covariances are described using Gaussian probability density functions (PDFs) with 0 mean error. Non-Gaussian PDFs due, for example, to nonlinear observation operators, are permitted using an appropriate nonquadratic version of (1) (e.g., Dharssi et al. 1992). Correlations between observation and background errors are neglected in (1) as is typical in 3/4DVAR systems (Parrish and Derber 1992; Zou et al. 1997; Lorenc et al. 2000). The use of adjoint operations permits efficient calculation of the multidimensional gradient of the cost function.

Given a model state $\mathbf{x}$ with n degrees of freedom (number of grid points times number of independent variables), calculation of the full background J^b term of (1) requires $\sim O(n^2)$ calculations. For a typical NWP model with $n^2 \sim 10^{12}$–10^{14} direct solution is not feasible in the time slot allotted for data assimilation in operational applications. One practical solution to reduce computational cost is to calculate J^b in terms of *control variables* defined via the relationship $\mathbf{x}' = \mathbf{U}\mathbf{v}$, where $\mathbf{x}' = \mathbf{x} - \mathbf{x}^b$ is the analysis increment. The $\mathbf{U}$ transform is designed to nondimensionalize the variational problem and also to permit use of efficient filtering techniques that approximate the full background error covariance matrix. If the $\mathbf{U}$ transform is well designed, condition numbers will be small and the product $\mathbf{U}\mathbf{U}^{\mathrm{T}}$ will closely match the full background error covariance matrix $\mathbf{B}$. In terms of analysis increments, (1) may then be rewritten

$$\begin{aligned} J(\mathbf{v}) &= J^b + J^o \\ &= \frac{1}{2}\mathbf{v}^{\mathrm{T}}\mathbf{v} + \frac{1}{2}(\mathbf{y}^{o'} - \mathbf{H}\mathbf{U}\mathbf{v})^{\mathrm{T}}(\mathbf{E} + \mathbf{F})^{-1}(\mathbf{y}^{o'} - \mathbf{H}\mathbf{U}\mathbf{v}), \end{aligned} \quad (2)$$

where $\mathbf{y}^{o\prime} = \mathbf{y}^o - H(\mathbf{x}^b)$ is the innovation vector and $\mathbf{H}$ is the linearization of the observation operator H used in the calculation of $\mathbf{y}^{o\prime}$.

a. Control variable transforms

In reality, the background error covariance matrix $\mathbf{B}$ may be synoptically dependent. The introduction of

so-called errors of the day in 3DVAR is possible via, for example, semigeostrophic grid transformations (Desroziers 1997), additional control variables, and anisotropic recursive filters (Purser et al. 2003b). In 4DVAR, flow-dependent structure functions are implicit through the use of the forecast model as part of the analysis solution [although a climatological estimate of background error is still applied in the calculation of J^b (Rabier et al. 2000)]. Nonvariational data assimilation systems, for example, ensemble Kalman filter methods (Houtekamer and Mitchell 1998; Anderson 2001) implicitly calculate ensemble-based estimates of flow-dependent forecast error as part of the solution. In the application-driven work described here, resources (both computational and human) permit only the specification of a climatological estimate for the background error covariance $\mathbf{B}$.

The ''NMC method'' (Parrish and Derber 1992) provides a climatological estimate of $\mathbf{B}$ assuming it to be well approximated by averaged forecast difference (e.g., month-long series of 24-h minus 12-h forecasts valid at the same time) statistics:

$$\mathbf{B} = \overline{(\mathbf{x}^b - \mathbf{x}^t)(\mathbf{x}^b - \mathbf{x}^t)^{\mathrm{T}}} = \overline{\boldsymbol{\varepsilon}_b \boldsymbol{\varepsilon}_b^{\mathrm{T}}} \sim \overline{[\mathbf{x}^f(T + 24) - \mathbf{x}^f(T + 12)][\mathbf{x}^f(T + 24) - \mathbf{x}^f(T + 12)]^{\mathrm{T}}}. \quad (3)$$

Here, $\mathbf{x}'$ is the true atmospheric state and $\boldsymbol{\varepsilon}_b$ is the background error. The overbar denotes an average over time and/or space. The resolution and variable dependence of the NMC method estimate for $\mathbf{B}$ is studied later for the triple-nested, two-way nesting domains of the Taiwanese MM5-based AOAWS. The NMC method estimate of $\mathbf{B}$ may also be tuned by comparing with independent estimates from accumulated observation minus background ($O - B$) data (Hollingsworth and Lönnberg 1986). Time variation of $\mathbf{B}$ is here limited to the calculation of error statistics for individual months/seasons.

The 3DVAR control variable transform $\mathbf{x}' = \mathbf{U}\mathbf{v}$ is implemented through a series of operations $\mathbf{x}' = \mathbf{U}_p\mathbf{U}_v\mathbf{U}_h\mathbf{v}$ (Lorenc et al. 2000). Each stage of the control variable transform is discussed in detail in Barker et al. (2003). The following is a summary.

The horizontal transform $\mathbf{U}_h$ is performed using *recursive filters* (Hayden and Purser 1995; Purser et al. 2003a). A recursive filter, rather than the spectral decomposition of Lorenc et al. (2000), is employed in order to facilitate the inclusion of anisotropic, inhomogeneous (flow-dependent) error correlations in future versions—spectral techniques are inherently homogeneous. The version of the recursive filter used here possesses only two free parameters for each control variable: the number N of applications of the filter ($N = 2$ defines a second-order autoregressive (SOAR) function response, as $N \to \infty$ the response approximates a Gaussian) and the correlation length scale s of the filter. A value of $N = 6$ is used in all applications. In experiments, this was the minimum number of passes required to remove unphysical ''lozenge''-shaped correlations in the wind field.

The background error correlation length scale s is specified for each variable and for each vertical mode. Length scales are estimated using the NMC method's accumulated forecast difference data processed as a function of gridpoint separation. A least-squares fit of the resulting curve to a Gaussian function is then used to estimate recursive filter length scales. The variable vertical and resolution dependence of s is illustrated in Fig. 2 for the 135- and 45-km domains of the AOAWS for 1 month (March 2000). There is a clear reduction in s for the 45-km domain relative to the 135-km domain. This is expected from differences seen in subjective comparisons of individual 24-h minus 12-h forecast difference fields (not shown) for 135- and 45-km domains. A valid question is whether the small-scale forecast differences truly represent background error features or are due to artifacts of the numerical forecasts, for example, boundary conditions, noise, etc. Indeed, a comparison of length scales calculated via the NMC method and using observation minus background differences has been performed, indicating some disparity in length scale estimates. Empirical multiplicative tuning factors are therefore applied to the length scales calculated via the NMC method (ranging between 0.5 and 1 depending on domain, variable). Further details will be given in a future paper. Also seen in Fig. 2 is a general trend of increasing length scale as a function of decreasing pressure—representing the dominance of synoptic-scale errors away from the boundary layer. The smaller-scale nature of humidity and wind errors relative to pressure and temperature fields is noticeable (except in the stratosphere). Tropopause effects are seen in temperature scales.

The vertical transform $\mathbf{U}_v$ is applied via an empirical orthogonal function (EOF) decomposition of the vertical component of background error $\mathbf{B}_v$ on model levels k where $\mathbf{B}_v$ is a $K \times K$ positive-definite, symmetric matrix (K = number of model levels). Given a domain/time-averaged estimate of $\mathbf{B}_v$ (via the NMC method), an eigendecomposition $\mathbf{B}_v = \mathbf{E}\Lambda\mathbf{E}^{\mathrm{T}}$ is performed to compute eigenvectors $\mathbf{E}$ and eigenvalues Λ. The vertical transform $\mathbf{U}_v$ is then given by $\mathbf{v}_p = \mathbf{U}_v\mathbf{v}_v = \mathbf{E}\Lambda^{1/2}\mathbf{v}_v$ that projects control variable space analysis increments $\boldsymbol{v}_v$ onto structures $\boldsymbol{v}_p$ on model levels.

The first eigenvector for each control variable is shown in Fig. 3 for each of the three nested MM5

TABLE 1. Impact of truncating 3DVAR's vertical modes ($M < K = 31$) to filter trailing eigenvectors responsible for only 0.1% of error variance. Results from a test 73 × 91 × 31 domain using Mar 2000 NMC-method statistics.

Variance (%)	M (ψ)	M (χ)	M (p_u)	M (q)	n	Iterations	J (final)	CPU (s)	Memory (Mbytes)
99.9	17	17	10	22	43 8438	25	1.33	251	220
100	31	31	31	31	82 3723	24	1.32	420	316

AOAWS domains using March 2000 data. Results are qualitatively similar to those presented in Ingleby (2001, his Fig. 7) for global data from the U.K. Met Office's ''Unified Model.'' The leading streamfunction eigenvector (40%; 42%, 36% of total 135-, 45-, 15-km error) peaks at jet levels (especially at lower resolution) consistent with errors in the nondivergent, intense winds expected at jet levels. The leading velocity potential eigenvector (41%, 51%, 56% of total 135-, 45-, 15-km error) indicates a strong signal from errors in the divergent wind in the boundary layer, negatively correlated with divergent wind errors in the middle-upper troposphere. The vertical component of error in unbalanced pressure is dominated by the first mode that accounts for 65%, 70%, 71% of the total climatological error in the 135-, 45-, 15-km domains, respectively. The error represents a pressure error correlation extending through much of the troposphere. This will result in the 3DVAR propagation of surface pressure observation information far into the middle troposphere (see later). There is little resolution dependence in the fraction of total specific humidity error explained by the first mode (50%, 51%, 51% of total 135-, 45-, 15-km error) and has a maximum magnitude at ~800 hPa. As with the horizontal length scales discussed previously, the shallow nature of the leading humidity mode is consistent with the smaller-scale nature of humidity relative to wind and mass variables. Finally, there is little dependence of any of the leading eigenvectors of vertical background error on horizontal resolution, with the possible exception of upper-level velocity potential error—the negative correlation between stratosphere and troposphere of the dominant 135-km mode in Fig. 3b (due potentially to the imposition of zero integrated mass divergence in the forecast model) is significantly exaggerated relative to the corresponding higher-resolution 45- and 15-km structures. Comparison of Figs. 7 and 8 of Ingleby (2001) indicates little difference between dominant global and tropical velocity potential vertical modes (calculated using a global model). This is evidence that the differences seen here may not be due to the larger region encompassed by the 135-km domain, but instead may be an effect of resolution and/or boundary conditions. Further investigations are necessary to provide a more complete answer to this question.

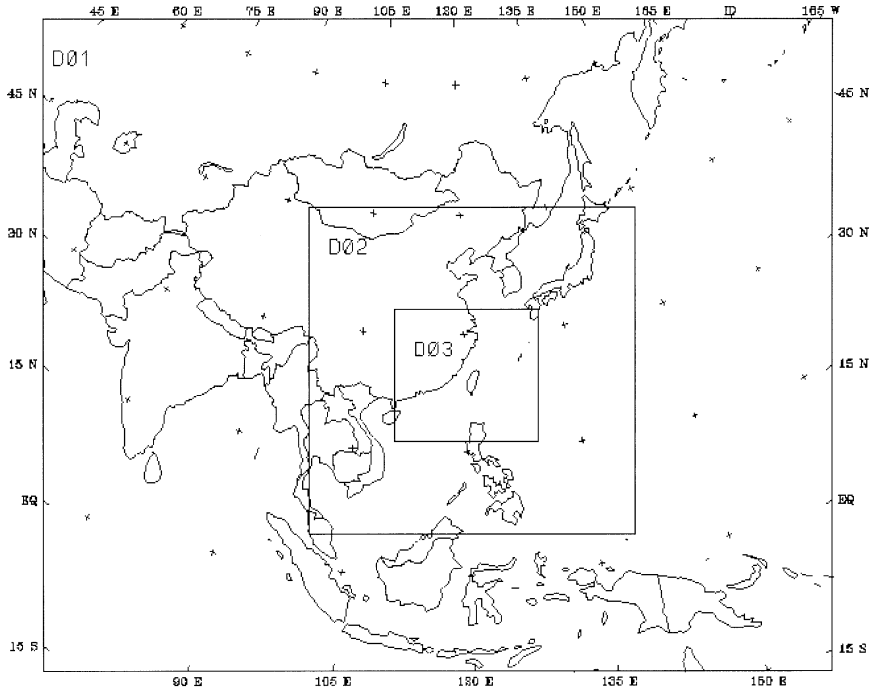

FIG. 1. The 135-, 45-, and 15-km nested domains of the MM5-based AOAWS system. 3DVAR is used in all three domains to initialize MM5 two-way nesting forecasts.

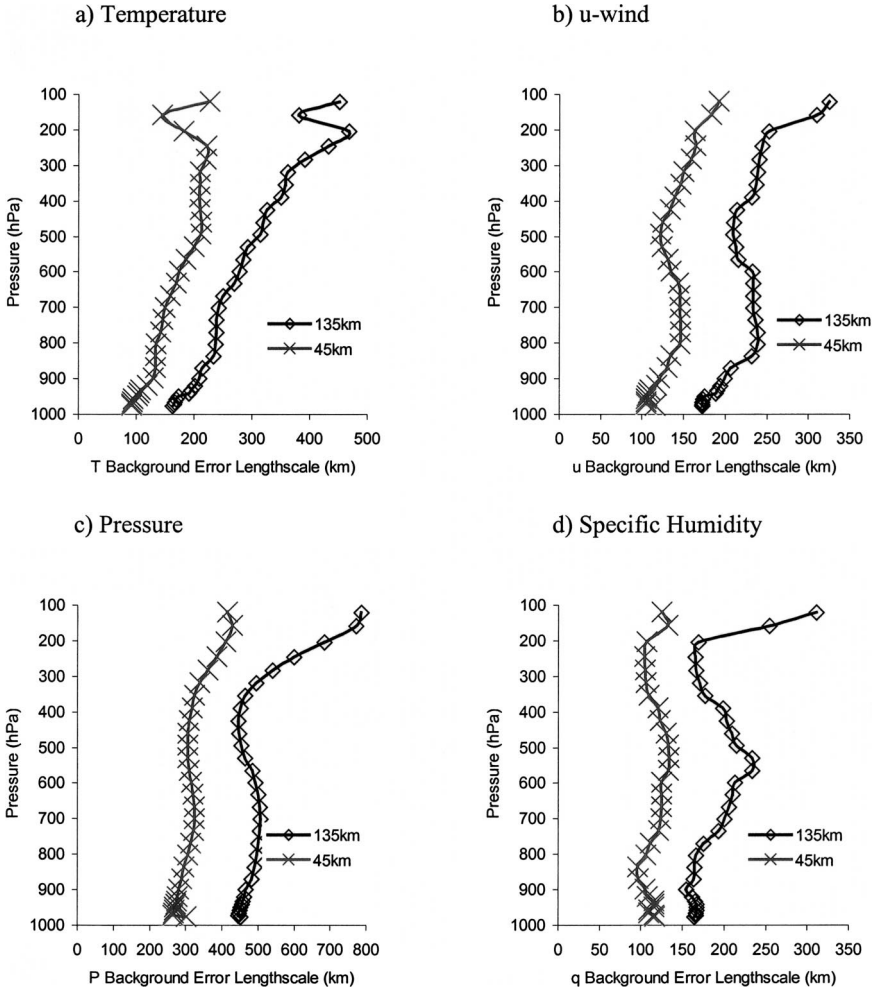

FIG. 2. Model space climatological estimates of background error length scale s for 135-, and 45-km AOAWS domains. (a) Temperature, (b) u-wind, (c) pressure, and (d) specific humidity. Scales are used (calculated in control variable space) in 3DVAR's recursive filters.

The projection onto orthogonal eigenvectors reduces the number of calculations required in the $\mathbf{U}_v$ transform from $O(K^2)$ to $O(K)$. By definition, the leading eigenvector ($m = 1$) contains the largest contribution to the background error. Trailing eigenvectors contain the least information and may be removed to reduce the computational cost of 3DVAR. Table 1 illustrates this for a sample 3DVAR analysis performed on a 73 × 91, 31-level test domain. Using all modes ($M = K = 31$), the minimization problem has 823 732 (73 × 91 × 31 × 4) degrees of freedom. 3DVAR convergence requires 24 iterations and uses 420s CPU and 316 Mbytes memory on NCAR's ''blackforest'' IBM SP-2 computer. Truncation of vertical modes to retain 99.9% of the background error variance results in a significant reduction in CPU (40%) and memory (30%) requirements. As expected, there is little impact on the final results (iterations and final cost function are very similar). The truncation of vertical modes therefore results in a significant cost reduction with negligible scientific impact.

The physical variable transformation $\mathbf{U}_p$ involves the conversion of control variables (ψ, χ, $_u$, and q) to model variable (u, v, T, p, q) increments. The recovery of pressure p is achieved via the relation $p = p_u + Cp_b$ where the linearized ''balanced'' pressure p_b on a model surface η is given by

$$\nabla^2_\eta p_b = -\nabla_\eta \cdot \overline{\rho}(\overline{\mathbf{v}} \cdot \nabla_\eta \mathbf{v}' + \mathbf{v}' \cdot \nabla_\eta \overline{\mathbf{v}} + f\mathbf{k} \times \mathbf{v}'). \quad (4)$$

The inclusion of the cyclostrophic terms [first two in brackets on rhs of (4)] is unique to this implementation of 3DVAR and permits an improved balance in regimes of high curvature (e.g., hurricanes). Variables $\overline{\rho}$ and $\overline{\mathbf{v}}$ represent the mean-field (background) state density and velocity fields respectively. Equation (4) is solved via a spectral (fast double sine transform) methods. If only geostrophic mass/wind balance were imposed, it would be simpler to derive a balanced wind from the mass gradient. However, a more sophisticated balance equation, for example, (4) is easiest to formulate if balanced mass increments are derived from wind increments. As

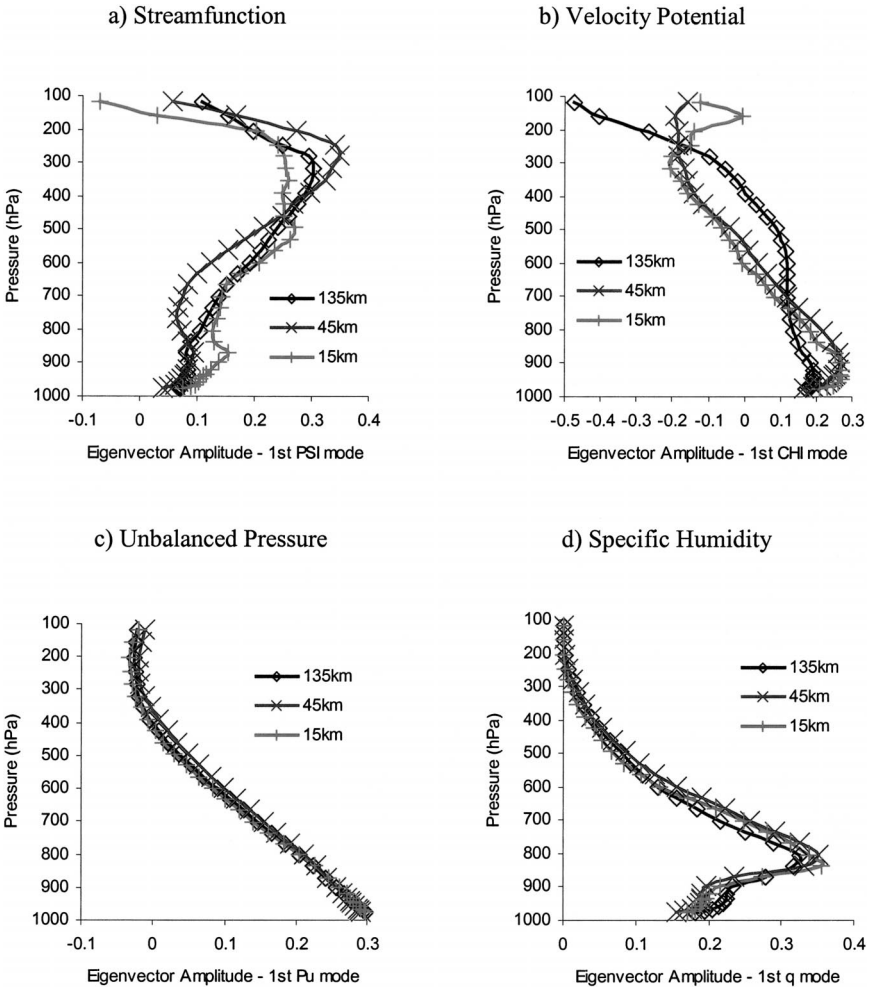

FIG. 3. First eigenvector ($m = 1$) of the vertical component of time–domain-averaged background error covariance matrix for (a) streamfunction, (b) velocity potential, (c) unbalanced pressure, and (d) specific humidity. The leading mode is plotted for each domain of the triple-nested AOAWS MM5 application. Mar 2002 forecast difference data used.

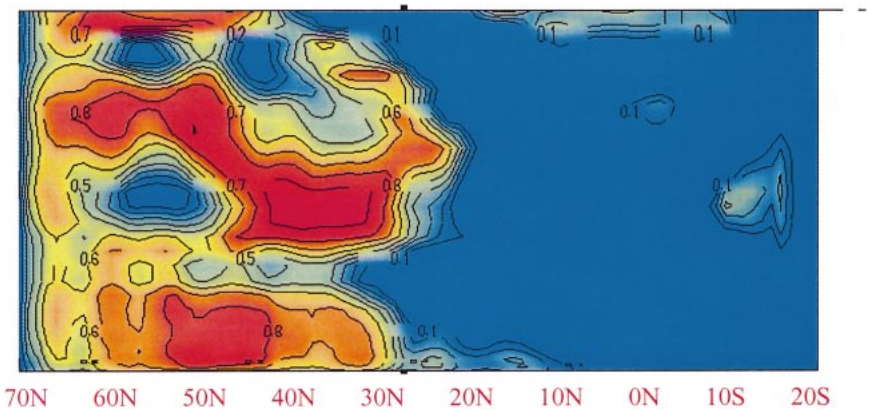

FIG. 4. Correlation between pressure increment and ''balanced'' pressure [derived from wind increments using (4)]. Horizontal axis is model y direction (approximate latitudes indicated). Vertical axis is model level (surface to 50 hPa, linear in pressure).

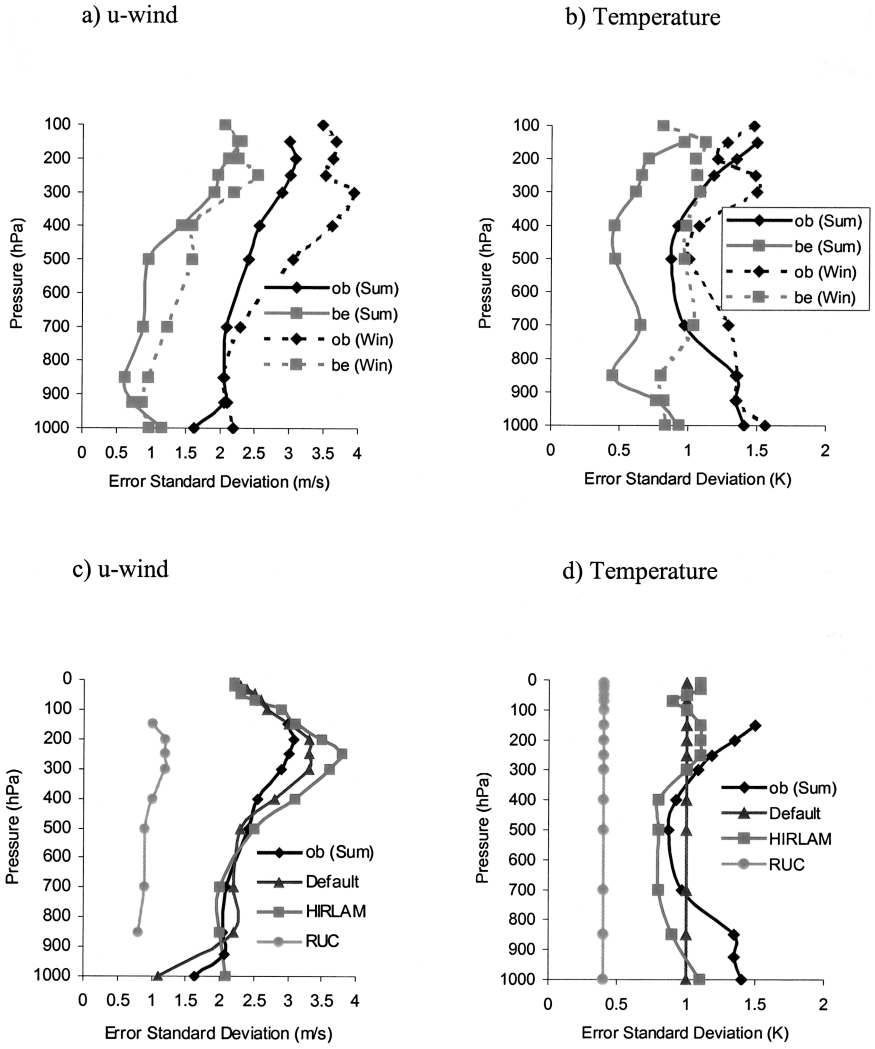

FIG. 5. Observation and background error variances as calculated from accumulated winter and summer AOAWS domain 2 $O - B$ data: (a) u-wind, (b) temperature. Comparison of observation errors used in HIRLAM, RUC, and MM5 (default and ''summer tuned'') 3DVAR systems: (c) u-wind, (d) temperature.

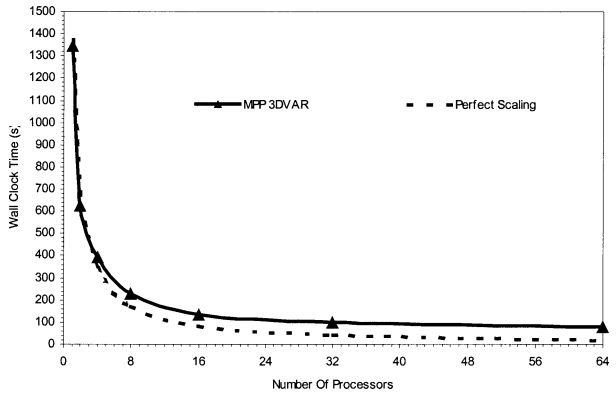

FIG. 6. Wall-clock time for test 3DVAR run in AFWA's 140 × 150 × 41 45-km ''T4'' domain—25 Jan 2002 case study. Times shown are for runs on NCAR's IBM SP-2 ''blackforest,'' with Winterhawk II nodes.

well as allowing the introduction of the cyclostrophic term, this formulation allows future experimentation with more sophisticated balance equations, for example, including the effects of friction, diabatic heating, etc.

The balanced pressure's regression coefficient C provides a statistical filtering of the p_b increment in regions where the balance equation (4) is not appropriate (e.g., Tropics). In these regions, the mass/wind analyses are partially decoupled. Figure 4 plots the correlation between pressure and balanced pressure p_b increments using 24-h minus 12-h wind and pressure forecast differences data as increments. One month (March 2000) MM5 forecast difference data is used from the 135-km domain of the AOAWS and is averaged over time and the x-direction. The resulting y–z section gives an indication of the regimes in which 3DVAR's mass/wind balance given by (4) is filtered. For example, the low

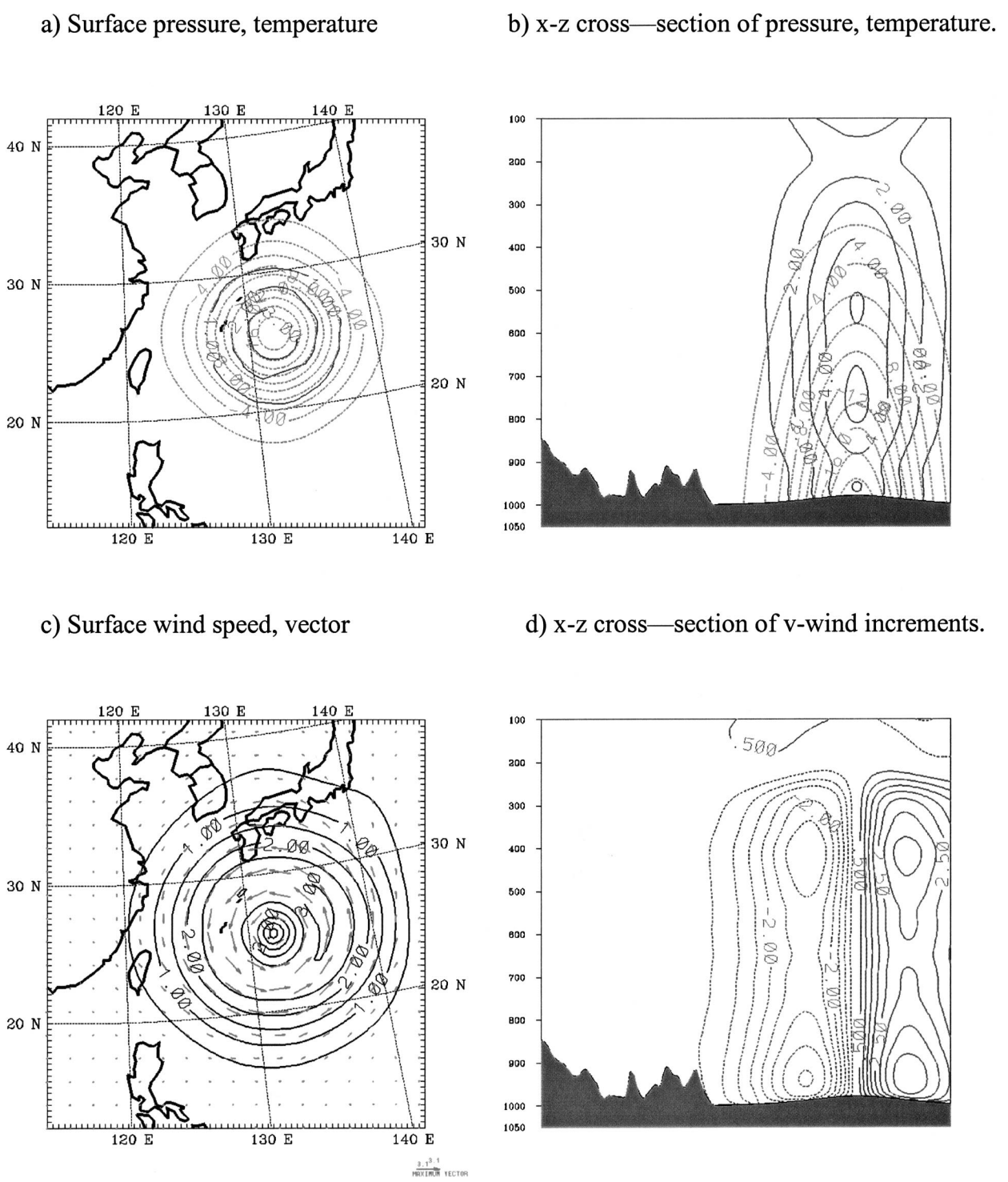

FIG. 7. 3DVAR's analysis increment response to bogus surface pressure observation. Pressure (negative, dashed) and temperature: (a) surface, (b) vertical *x*–*z* cross section. (c) Surface wind speed/vectors, (d) vertical *x*–*z* cross section though observation location for *v*-wind component.

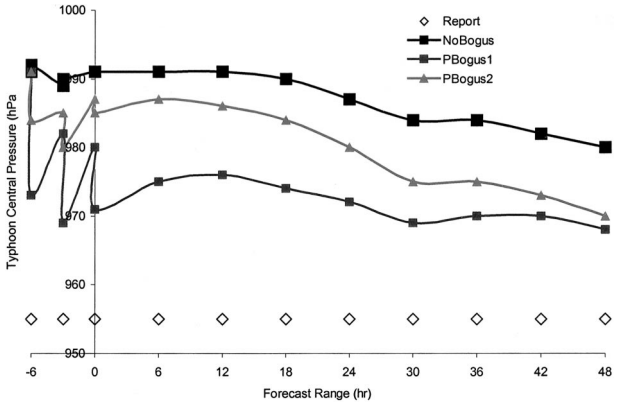

FIG. 8. The 48-h (0000 UTC 4 Sep–0000 UTC 6 Sep 2002) surface central pressure forecasts for Typhoon Sinlaku. Initial −6 to 0 h 3-hourly 3DVAR/MM5 cycling period also shown. Constant 955-hPa ''report'' values are from CWB typhoon warning reports.

correlation in the Tropics are consistent with the breakdown of geostrophic balance at low latitudes. The low correlation near the northern boundary (70°N) is an artifact of using a fast sine transform ($p_b = 0$ at boundaries) in the solution of (4) and should not be used to infer geostrophic balance is not appropriate at these latitudes (which it is). These effects mean that filtering of the balanced pressure increments is crucial.

b. Observation preprocessing and quality control

Observations available over the global telecommunications system (GTS) originate from a wide variety of sources. Errors may be introduced at all stages including measurement, reporting practices, transmission, and decoding. It is essential that careful quality control (QC) be performed to avoid the assimilation of erroneous observations.

An observation preprocessor has been developed to perform QC of observations. A number of checks are performed including removal of observations outside the domain, excluding location/time duplicates and incomplete observations (e.g., no location), and ensuring vertical consistency of upper-air profiles. Numerous QC checks are redone in 3DVAR itself and an ''error_max'' check performed to reject observations whose innovation vector ($O - B$) is greater than 5 times the assumed observation error standard deviation.

c. Background error tuning

As discussed earlier, the NMC method provides only an approximation to the climatological component of background error. Similarly, estimates of observation errors, supplied in tables from AFWA, may be inaccurate for a given observation type and resolution. Ideally, representiveness error should be tuned for each resolution domain and for synoptic situation since strong local gradients are likely to significantly increase this component of error. In this section, only a single example of tuning is performed.

In this section, results are presented of observation/background error variance estimates derived from accumulated east Asian radiosonde observation minus background ($O - B$) differences processed according to Hollingsworth and Lönnberg (1986). In this method, $O - B$ station pair correlations are binned as a function of station separation. Given sufficient data, the resulting distribution can be used to estimate climatological, isotropic background error covariances as well as observation error variances. Error estimates from $O - B$ data are used to further tune both background and observation errors used in 3DVAR. A future paper will describe a more extensive application of this tuning together with a complementary ''variational cost function diagnostic'' tuning method (Desroziers and Ivanov 2001) using high-density surface observations.

Data is collected from the operational AOAWS for summer (June–August 2001) and winter (December 2001–February 2002) seasons. In the AOAWS system, lateral boundary conditions for the largest domain are taken from the Taiwan Central Weather Bureau's (CWB's) global model. MM5 forecasts are generated every 3 h and are integrated out to 48 h using 3DVAR initial conditions computed in ''intermittent cycling'' mode. In this setup, 3DVAR's background at 0000 and 1200 UTC is the CWB's global analysis, whereas for the other initializations (0300, 0600, 0900, 1500, 1800, 2100 UTC) the background is a 3-h MM5 forecast. Only ''cold-starting'' data is used in this tuning study, that is, observations valid at 0000/1200 UTC.

Estimates of radiosonde observation and collocated background error variances derived from the $O - B$ data for selected pressure levels are given in Figs. 5a,b. For both wind and temperature, observation errors are larger than background errors. This is consistent with the fact that the ''background'' for 3DVAR at 0000/1200 UTC is an analysis (which has already assimilated an unknown number of conventional observations at relatively low resolution). Thus, the MM5 3DVAR analysis ''believes'' the background more than the observations ($\sigma^b < \sigma^o$) and hence produces only small analysis increments. This conservative approach limits potential problems of overfitting conventional observations due to assimilating the same observations twice (in background and 3DVAR analyses). The role of nested 3DVAR in cold-start mode is to ''add value'' through the introduction of new and/or high-resolution observations. It should be noted that the use of an analysis as a background field reduces the validity of the assumption of uncorrelated background and observation errors, used in both the 3DVAR cost function (1) and in the error tuning described in this section. Given the final product of our tuning, the observation error variances seen in Fig. 5, agree reasonably well with those used in models (which use very different background

fields), it can be argued that the tuning is not adversely affected by this assumption.

The cold-starting application described in this paper is a preliminary step towards full-cycling 3DVAR, in which the background field is a short-range forecast and hence its errors should be less correlated with those of the observations. Other motivations for cycling 3DVAR include (i) the inclusion of higher-resolution detail in the first guess field, (ii) a reduction in spinup problems as the first guess and subsequent forecasts are derived from the same numerical model, (iii) tighter control (number, type, quality) of observations assimilated.

Figure 5 indicates a general increase in both observation and background errors in winter relative to summer. Thus the processing of observation minus forecast statistics can be used to introduce seasonal error tuning factors for both observation and background error.

Comparison of observation errors used in other models offers a check on the error values produced from the $O - B$ data. Figures 5c and 5d illustrate the comparison for wind and temperature errors from the 45-km AOAWS domain. The ''default'' values are specified in tables compiled from NCEP/AFWA values. The $O - B$ estimates errors ''ob (Sum)'' are consistent with high-resolution limited-area model (HIRLAM) errors [representiveness error is applied separately in the Rapid Update Cycle (RUC) 3DVAR (D. Devenyi 2002, personal communication) explaining the small RUC values]. The $O - B$ estimates of radiosonde temperature errors also contain a more realistic variation with pressure than the default values. The agreement with observation error estimates used in independent models supports the validity of the $O - B$ error estimation method. In turn, this validates the background error values seen in Figs. 5a and 5b as the observation errors are calculated as a residual of the $O - B$ and background error variances (Hollingsworth and Lönnberg 1986).

d. Computational optimization

A major effort has been to develop a distributed memory (DM) capability for 3DVAR using software designed for the Weather Research Forecast model (Michalakes et al. 2001). The 3DVAR system contains a number of algorithms that pose new challenges to the WRF software architecture for running on DM systems. First, the specification of background error covariances via recursive filters and the use of fast sine transforms in 3DVAR's balanced pressure calculation (4) requires a domain decomposition along the entire domain (both north–south and east–west). Second, the minimization algorithm requires the parallelization of large vector dot-products. Finally, the inhomogeneous nature of the observation network ideally requires an irregular horizontal domain decomposition (although a regular decomposition is currently used).

The DM speedup achieved running 3DVAR with differing numbers of processors on NCAR's IBM-SP blackforest machine is shown in Fig. 6. The case used is valid at 1200 UTC on 25 January 2002 in AFWA's 45-km southwest Asian ''T4'' $140 \times 150 \times 41$ domain. Minimization in this case is achieved in 98 iterations. For this case, wall-clock time for single-processor 3DVAR is 1373 s reducing to 115 s using 64 processors. Tuning of background error variances and length scales reduces the number of iterations to convergence from 98 to 49. Although 3DVAR is far from scalable above 16 processors—compare ''perfect'' scaling with actual in Fig. 6—the resulting wall-clock time of 58 s is well within the AFWA operational time-window and is significantly faster than the DM MVOI system it replaces (M. McAtee 2002, personal communication). Further parallelization may be required in future if the cost of 3DVAR increases considerably, for example, through the introduction of radiances, larger domains, etc.

The DM 3DVAR code has been tested on a number of machines including DEC, IBM-SP, Fujitsu VPP5000, SGI, PC/LINUX, and Alpha/LINUX platforms. Standard tests performed after each major release include adjoint–inverse correctness checks, single observation tests, selected case-study impact, cross-platform checks, and impact of differing numbers of processors. As well as outputting the analysis and (optionally) the analysis increment files, multiple diagnostics are computed, including observation usage details, the background forecast/analysis fit ($O - B$, $O - A$) to individual observation types, analysis increment statistics, and cost function/gradient minimization information.

3. 3DVAR single observation test: Application to typhoon bogusing

In this section, the multivariate, three-dimensional nature of 3DVAR's background error covariances is examined by studying 3DVAR's response to a single bogus surface pressure observation. Following this, the 48-h forecast impact of the bogus observation on the track and intensity of a typhoon is presented. The typhoon chosen for this case study is Sinlaku, which made landfall in southeast China in the first week of September 2002. The AOAWS 3DVAR/MM5 implementation (described earlier) is used.

The 3DVAR analysis increment response at 1800 UTC 3 September 2002 to a single bogus surface pressure observation of 955 hPa at location (25.6°N, 132.0°E) is shown in Fig. 7. At this time, the background is a 6-h, 45-km-resolution MM5 forecast taken from the operational AOAWS. Bogus central pressure and location estimates are taken from CWB typhoon reports (based on human interpretation of satellite imagery). In reality, the typhoon is unlikely to maintain the constant value of 955 hPa over a 48-h period (see Fig. 8) as estimated in the report. In this experiment, we represent this uncertainty using two different estimates (1 hPa, 2 hPa) of the observation error assigned to the bogus observation.

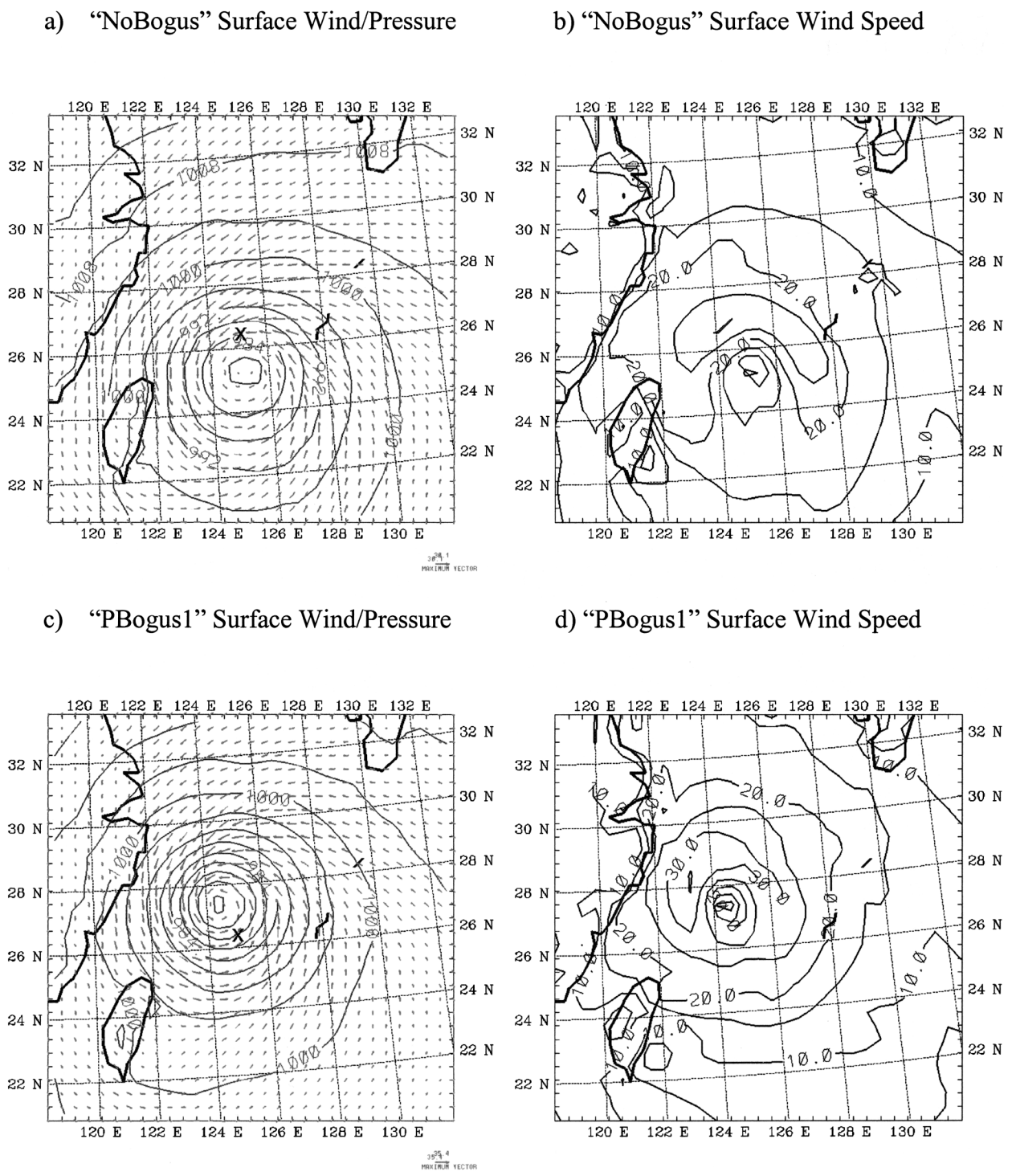

FIG. 9. The 48-h forecasts of Typhoon Sinlaku valid at 0000 UTC 6 Sep 2002. Experiments (a), (b) NoBogus, (c), (d) PBogus1, and (e), (f) PBogus2. (left) Surface pressure (4-hPa contours) and wind vectors; (right) surface wind speed (5 m s^{-1} contours). Here, "X" is the typhoon's observed position.

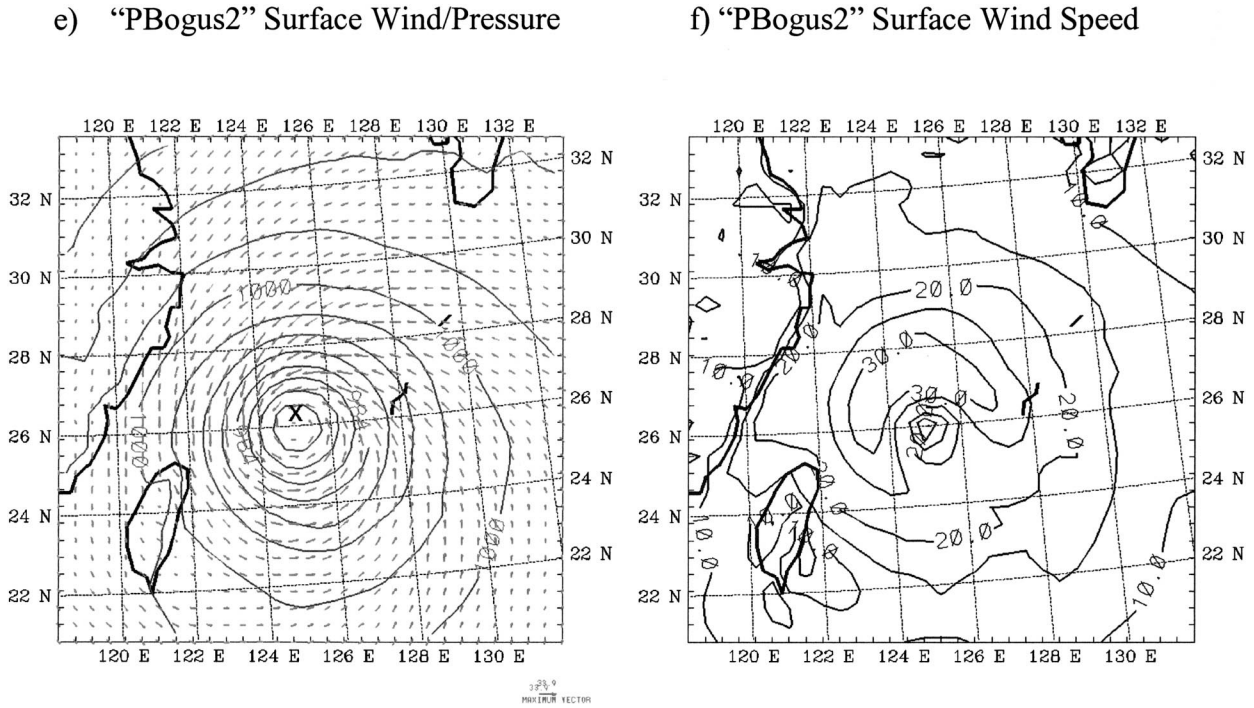

FIG. 9. (*Continued*)

The forecast typhoon surface central pressure at 1800 UTC 3 September is 991 hPa, that is, there is an observation minus background difference of 36 hPa (the usual QC check on maximum $O - B$ is suppressed for bogus observations). Using a bogus pressure observation error of 1 hPa (2 hPa), 3DVAR's surface pressure analysis is 973 hPa (984 hPa) at the typhoon location, that is, there is an 11-hPa difference in the analyzed central pressure. This large sensitivity is easily explained by a simple calculation of the gradient of the cost function (1) at minimum for a single observation y^o. The resulting analysis central pressure is given by

$$y = (\sigma_b^2 y^o + \sigma_o^2 y^b)/(\sigma_b^2 + \sigma_o^2). \quad (5)$$

Using $y^b = 991$ hPa, $y^o = 955$ hPa, $\sigma_b = 1$ hPa (derived from the NMC statistics) and $\sigma_o = 1$ hPa, leads to $y = 973$ hPa. Using the PBogus2 value of $\sigma_o = 2$ hPa gives $y = 984$ hPa.

The approximately circular pressure increment field (Fig. 7a) is a response to the observation of 3DVAR's currently isotropic recursive filters. The scale is determined by the background error length scales estimated via the NMC method (see section 2). The corresponding temperature increment is created via hydrostatic balance and the ideal gas law. The vertical cross section of p, T shown in Fig. 7b indicates that 3DVAR's EOF decomposition of background error propagates the surface information well into the upper troposphere. Surface cyclonic wind increments, consistent with 3DVAR's filtered geostrophic/cyclostrophic mass/wind balance (4), are clearly seen in Fig. 7c. The wind response (maximum $\sim$3 m s^{-1}) is significantly subgeostrophic as a result of the statistical filtering of balanced pressure increments described earlier. This conclusion follows from a simple calculation of the magnitude of the geostrophic wind $v_{\text{geo}} = 1/(\rho f)\partial p/\partial x \sim 63$ m s^{-1} given values of $\rho = 1$ kg m^{-3}, $f = 2\Omega \sin\phi = 6.3 \times 10^{-5}$ s^{-1} for latitude $\phi = 25°$, $\delta p = 20$ hPa, and $\delta x = 500$ km as estimated from Fig. 7a. Note the slight nonaxisymmetric component of the wind increment which is a result of the dependence of balanced pressure on the background wind field in (4). Figure 7d shows the vertical propagation of wind increments, again in approximate balance with the pressure field shown in Fig. 7b.

It should be emphasized that the background error covariances producing these structures are climatological averages and do not specifically represent the forecast errors associated with a particular typhoon (this will be possible using ''errors of the day'' in a later version of 3DVAR). The dependence on the background state in (4) does introduce some case-dependence and using more than one observation will also help to define the structure. Despite this, the current 3DVAR will produce a similar response to different typhoons that may in reality have very different structures. However, the current 3DVAR increments propagate the observed data in a climatologically and dynamically consistent way.

Attention is now turned to the impact of analysis increments on the subsequent forecast evolution of the typhoon. This short typhoon study is intended to investigate (a) the persistence of information from a single bogus surface pressure observation through the forecast when

assimilated using 3DVAR, and (b) the sensitivity of the typhoon track/intensity forecast to subtle changes in 3DVAR's usage of the single bogus observation. Forecasts are integrated for 48 h from analyses valid at 0000 UTC 4 September 2002 following two initial 3DVAR/3-hr-MM5 spinup cycles 1800–2100 UTC, 2100–0000 UTC). Three experiments are performed.

- NoBogus: Standard observations—Surface, TEMP, SATEM, SATOB, AIREP, Quikscat.
- PBogus1: NoBogus + Surface pressure bogus (P = 955 hPa, error = 1 hPa).
- PBogus2: NoBogus + Surface pressure bogus (P = 955 hPa, error = 2 hPa).

Typhoon central pressure values through the forecast are presented in Fig. 8. The ''saw-tooth'' appearance in the −6 to 0 h range of Fig. 8 indicates the 3-h cycling MM5 forecast is reacting to the introduction of the bogus observation in 3DVAR. Two cycles are clearly insufficient to remove this spinup completely. Without the bogus pressure observation, the ''NoBogus'' forecast gradually deepens through the period from an initial value of 991 to 980 hPa at 0000 UTC on 6 September. The ''PBogus1'' and ''PBogus2'' curves indicate that the impact of the pressure observation is retained throughout the 48-h forecast in both bogus experiments resulting in 48-h forecast typhoon central pressures of 968–970 hPa for PBogus1–PBogus2 experiments—respectively, 23/21 hPa lower than the NoBogus forecast.

Figure 9 presents 48-h MM5 forecasts of Typhoon Sinlaku valid at 0000 UTC 6 September 2002. The actual position of the typhoon at this time is denoted ''X.'' Figures 9a and 9b correspond to the NoBogus experiment and indicate that in addition to insufficient deepening, the forecast typhoon is misplaced ~130 km to the south. In addition to the deepening of the typhoon, the 3DVAR assimilation of the surface bogus observation also modifies the track of the typhoon. The stronger pull to the bogus observation of PBogus1 results in a typhoon position ~260 km north of that of NoBogus (a positioning error of 130 km to the north) as seen in Figs. 9c and 9d. The larger observation error applied in PBogus2, results in a 48-h typhoon that is only ~50 km from the true position as seen in the Figs. 9e and 9f.

The right-side panels in Fig. 9 indicate a maximum surface wind speed in the leading right edge of the typhoon path. Maximum surface wind speeds are 30.1, 35.4, 33.9 m s^{-1} for experiments NoBogus, PBogus1, and PBogus2, respectively.

The conclusions drawn from this preliminary study are: (a) the impact of 3DVAR assimilation of a bogus surface pressure observation does persist through the forecast, and (b) there is significant sensitivity of the typhoon forecast (particularly the track) to the way the bogus observation is assimilated in the 3DVAR initial conditions.

4. Verification from real-time AOAWS system

Initial real-time deployment of the 3DVAR system built for MM5 has been geared towards implementations in the AOAWS and AFWA MM5-based systems. A future paper will describe encouraging verification results from initial AFWA implementations of 3DVAR. In this section, results from the implementation of 3DVAR in the MM5-based on AOAWS are discussed. As in the initial AFWA implementation, no new observation types are assimilated—differences are due to those in the assimilation algorithm alone. Unfortunately, many of the observation types that the 3DVAR system can assimilate are not yet available in the AOAWS operational data stream. These observation types include SSM/I retrievals/radiances, Quikscat oceanic surface wind speed/direction, and Global Positioning System (GPS) total precipitable water (TPW). This limits the potential benefits of 3DVAR in the initial AOAWS implementation. Future work will assess the impact of these, and other, additional observations. In this paper, the comparison of 3DVAR against the previously operational ''LITTLE_R'' Cressman scheme (Cressman 1959) records the relative performance of these two schemes. This paper does not attempt to compare our 3DVAR formulation against alternative modern data assimilation techniques, for example, observation space 3DVAR (Cohn et al. 1998; Daley and Barker 2001), 4DVAR (Zou et al. 1997; Rabier et al. 2000), or ensemble Kalman filter techniques (Houtekamer and Mitchell 1998; Anderson 2001).

Forecast verification scores for the u-wind component are shown in Fig. 10 for the 135-, 45-, and 15-km AOAWS MM5 domains 1–3 (scores for the v-wind component are similar). Verification is against radiosonde observations. The period chosen is 1 week from 0000 UTC 2 September–0000 UTC 9 September 2002 using forecasts initialized at 0000/1200 UTC. The 3DVAR system is set up to cold-start from CWB global analyses at main synoptic hours (0000/1200 UTC) and to cycle MM5 at other times, that is, the first guess at intermediate 3-hourly cycles is a 3-h MM5 forecast. The ''NOOBS'' run is an MM5 forecast run from the interpolated CWB analysis. The 3DVAR improvement relative to NOOBS is a measure of the added value of the MM5 3DVAR reanalysis.

The analysis (T + 00) fit to observations is closer for LITTLE_R than for 3DVAR. As discussed earlier, in a situation where observation errors are larger than background errors a very close fit to observations at analysis time does not necessarily indicate a better analysis. The degradation of LITTLE_R accuracy relative to 3DVAR increases for domains 2 and 3 is clearly seen in Fig. 10. This may well be related to the Cressman scheme's increasing overfitting of observations for the smaller domains (a single observation is fitted exactly in the Cressman scheme). Using 3DVAR, the wind forecast verification is improved relative to LITTLE_R without the associated overfitting at T + 00 associated with LITTLE_R. The 3DVAR improvement in wind forecast is largest for

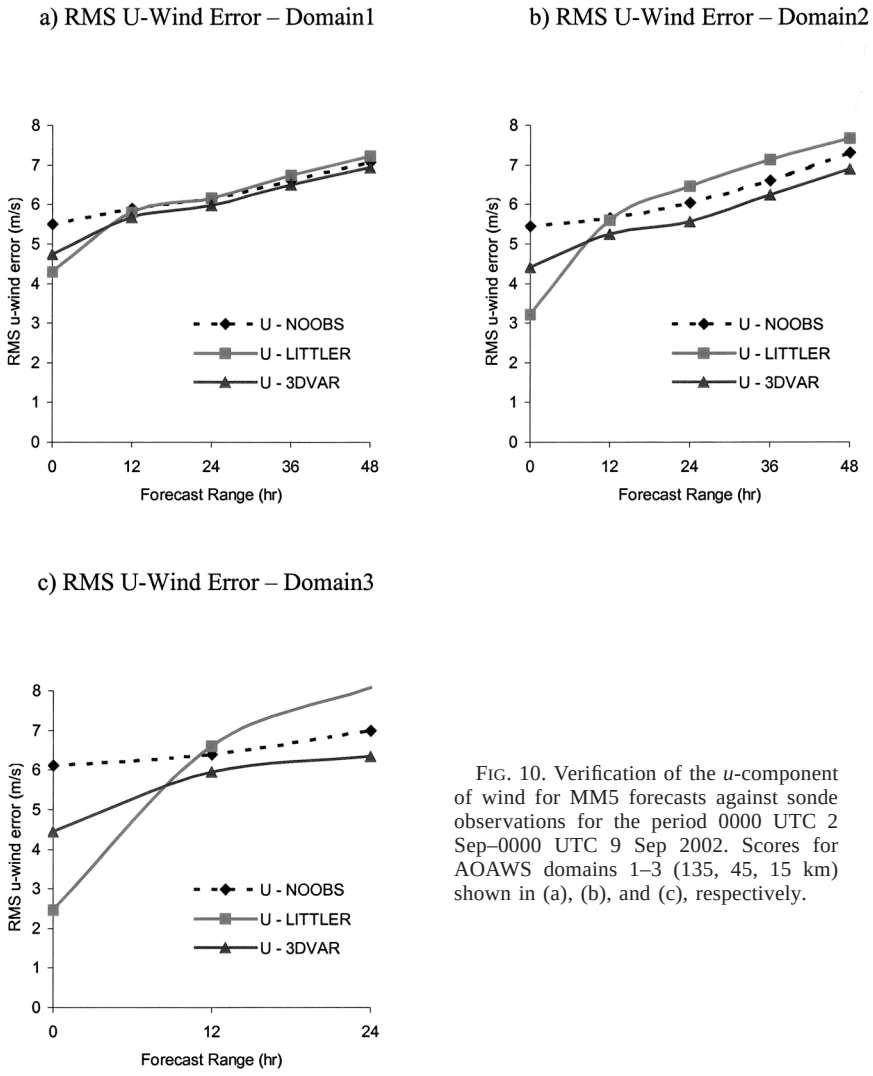

FIG. 10. Verification of the *u*-component of wind for MM5 forecasts against sonde observations for the period 0000 UTC 2 Sep–0000 UTC 9 Sep 2002. Scores for AOAWS domains 1–3 (135, 45, 15 km) shown in (a), (b), and (c), respectively.

the higher-resolution (15 km) domain 3 and extends to all forecast ranges.

Verification of temperature and moisture fields shown in Fig. 11 show only a small improvement in AOAWS forecast verification using 3DVAR (and indeed LITTLE_R) analyses. From Fig. 11, there is clearly a significant error in temperature and moisture in the initial conditions that dominates the subsequent forecast error growth so the assimilation procedure has a role to play in reducing forecast error. Work is currently under way to investigate this feature. One potential problem in the current code is the vertical interpolation in the observation operators from model levels to observation location as a function of height rather than pressure—a legacy of the MM5 height-based system. The actual observed vertical coordinate for many observation types (e.g., sondes) is pressure (height is currently derived from pressure introducing additional error). In preliminary studies this change has been shown to result in smaller observation increments ($O - B$) and fewer rejected observations. Further tests will investigate if the mass field analyses are more seriously degraded by this effect than the wind analyses.

AOAWS verification has been performed for numerous week-long periods over a 1-yr preoperational testing period. Results illustrated here are representative of the general conclusion that 3DVAR provides significant improvements in the forecast wind field, but only marginal impact on mass and moisture fields.

The 3DVAR system runs in ~5 min wall-clock time using nine processors for the three nested AOAWS domains on the Fujitsu VPP-5000 of CAA. This compares well with ~8 min wall-clock time for the LITTLE_R assimilation system running one processor/domain in parallel. Thus, the 3DVAR system provides improved forecasts (that will presumably get better still with the inclusion of additional observation types, for example,

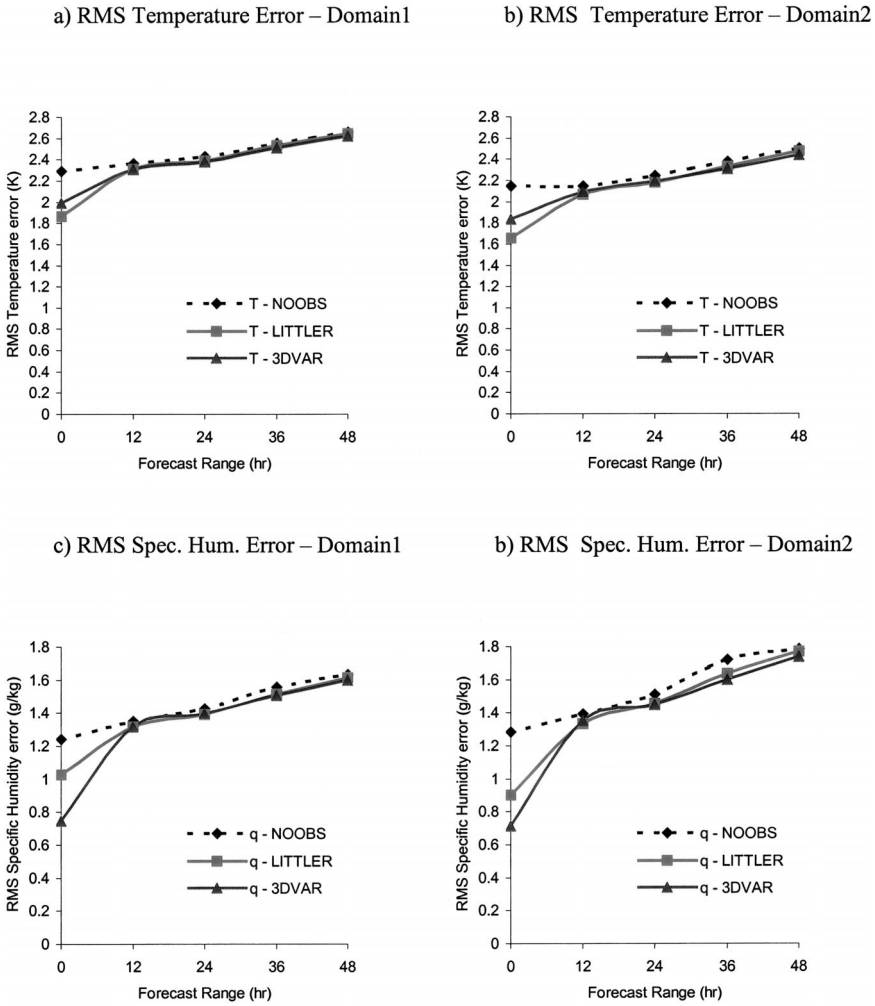

FIG. 11. (a),(b) Temperature and (c),(d) specific humidity forecast verification against sonde observations for AOAWS (left) 135-km domain 1 and (right) 45-km domain 2. Same period as in Fig. 10.

radiances that cannot be assimilated in the LITTLE_R system) in less wall-clock time than its predecessor at CAA.

5. Summary and conclusions

This paper describes the practical implementation of a 3DVAR system developed for the MM5 model and results from an initial case study and real-time applications. An overview of the system has been given—for further details see Barker et al. (2003). The truncation of eigenmodes of the vertical component of the background error covariance leads to computation savings of the order of 30%–40%. An assessment of the resolution dependence of errors in the background forecasts (using the NMC-method) using data from the two-way nesting, 135-, 45-, 15-km domains of the CAA's MM5-based AOAWS reveals detailed features, for example, variable length scales that are used within 3DVAR to impose detailed, multivariate background error covariances. The limitation of climatological background errors will be removed in the near future through the inclusion of anisotropic recursive filters.

A seasonal study of $O - B$ estimates of both background and observation error variances provides an independent estimate of climatological errors to those given by the NMC-method and observation error tables, respectively. Comparison of $O - B$ estimated errors indicate that in cold-start mode, where the background is already an analysis, a conservative approach should be taken in order to avoid overfitting observations. A future paper will describe the use of observation space diagnostics to tune a 3DVAR application in ''cycling'' mode.

Two examples of applications of the 3DVAR system to the MM5 model have been described. The three-dimensional, multivariate 3DVAR response to a single surface pressure observation is presented in the context

of a typhoon bogussing experiment. This simple application illustrates (a) 3DVAR's multivariate covariances, (b) the sensitivity of the analysis to prescribed bogus observation error, and (c) a significant impact of the bogus observation on the 48-h forecast track and intensity of the typhoon. Results are also presented from one of the two initial real-time applications of 3DVAR with MM5. A significant improvement in forecast wind scores is seen using 3DVAR in the AOAWS, especially for the higher-resolution domains. Temperature and humidity scores show only a marginal improvement. A future paper will describe forecast verification results from the AFWA implementation of 3DVAR, in which significant improvements in wind, mass, and moisture fields are found compared with forecasts from the previously operational MVOI system.

The practical implementation of 3DVAR using tuned background error statistics and truncated vertical error modes on distributed memory platforms results in a fast data assimilation system that runs efficiently and robustly in operational environments around the world (United States, Taiwan, and more recently Korea). A particular challenge has been to maintain this efficiency on a variety of computational platforms. Of course, this flexibility is a requirement for the code in the general research community. The 3DVAR system is freely available to the data assimilation research community (see http://www.mmm.ucar.edu/3dvar) and is already being used by the community in MM5 mode. For example, Cucurull et al. (2004) describe an application of the code to the case-study assimilation of ground-based GPS zenith total delay observations. Chen et al. (2003) describe the impact of the assimilation of SSM/I retrievals (total precipitable water, surface wind speed) and microwave radiances on the forecast evolution of Hurricane Danny.

Current NCAR 3DVAR efforts are geared towards the development of a 3DVAR system for WRF, starting from the 3DVAR code developed for MM5 described here. A ''basic'' version of WRF 3DVAR was released in June 2003. In addition, new observation types currently being included in 3DVAR include radar radial velocity and GPS radio occultation data (Kuo et al. 2000). As well as the obvious extension to 4DVAR for WRF, it is planned to use the observation preprocessing and operators developed for 3DVAR in the design of an ensemble Kalman filter capability for WRF (Anderson 2001).

Acknowledgments. The authors would like to thank Andrew Crook, Bill Kuo, Jordan Powers, and Chris Snyder for comments on an earlier version of this paper. Comments by two anonymous referees also improved the quality of the paper. We are grateful to the United States Weather Research Program, AFWA, and the Taiwanese CAA for supporting this work.

REFERENCES

Anderson, J., 2001: An ensemble adjustment Kalman filter for data assimilation. *Mon. Wea. Rev.,* **129,** 2884–2903.

Barker, D. M., W. Huang, Y.-R. Guo, and A. Bourgeois, 2003: A three-dimensional variational (3DVAR) data assimilation system for use with MM5. NCAR Tech. Note. NCAR/TN-453 + STR, 68 pp. [Available from UCAR Communications, P.O. Box 3000, Boulder, CO 80307.]

Chen, S. C., F. C. Vandenberghe, G. W. Petty, and J. F. Bresch, 2003: Application of SSM/I satellite data to a hurricane simulation. *Quart. J. Roy. Meteor. Soc.,* **132,** 749–763.

Cohn, S., A. da Silva, J. Guo, M. Sienkiewicz, and D. Lamich, 1998: Assessing the effects of data selection with the DAO Physical-Space Statistical Analysis System. *Mon. Wea. Rev.,* **126,** 2913–2926.

Courtier, P., J.-N. Thépaut, and A. Hollingsworth, 1994: A strategy for operational implementation of 4D-Var, using an incremental approach. *Quart. J. Roy. Meteor. Soc.,* **120,** 1367–1387.

Cressman, G. P., 1959: An operational objective analysis system. *Mon. Wea. Rev.,* **87,** 367–374.

Cucurull, L., F. C. Vandenberghe, D. M. Barker, E. Vilaclara, and A. Rius, 2004: Three-dimensional variational data assimilation of ground-based GPS ZTD and meteorological observations during the 14 December 2001 storm event over the western Mediterranean sea. *Mon. Wea. Rev.,* **132,** 749–763.

Daley, R., and E. Barker, 2001: NAVDAS: Formulation and diagnostics. *Mon. Wea. Rev.,* **129,** 869–883.

Desroziers, G., 1997: A coordinate change for data assimilation in spherical geometry of frontal structures. *Mon. Wea. Rev.,* **125,** 3030–3039.

——, and S. Ivanov, 2001: Diagnosis and adaptive tuning of observation-error parameters in a variational assimilation. *Quart. J. Roy. Meteor. Soc.,* **127,** 1433–1452.

Dharssi, I., A. C. Lorenc, and N. B. Ingleby, 1992: Treatment of gross errors using maximum probability theory. *Quart. J. Roy. Meteor. Soc.,* **118,** 1017–1036.

Dudhia, J., 1993: A nonhydrostatic version of the Penn State/NCAR Mesoscale Model: Validation tests and simulations of an Atlantic cyclone and cold front. *Mon. Wea. Rev.,* **121,** 1493–1513.

Hayden, C. M., and R. J. Purser, 1995: Recursive filter objective analysis of meteorological fields: Applications to NESDIS operational processing. *J. Appl. Meteor.,* **34,** 3–15.

Hollingsworth, A., and P. Lönnberg, 1986: The statistical structure of short-range forecast errors as determined from radiosonde data. Part I: The wind field. *Tellus,* **38A,** 111–136.

Houtekamer, P. L., and H. L. Mitchell, 1998: Data assimilation using an ensemble Kalman filter technique. *Mon. Wea. Rev.,* **126,** 796–811.

Ide, K., P. Courtier, M. Ghil, and A. C. Lorenc, 1997: Unified notation for data assimilation: Operational, sequential and variational. *J. Meteor. Soc. Japan,* **75,** 181–189.

Ingleby, N. B., 2001: The statistical structure of forecast errors and its representation in the Met. Office Global 3-D Variational Data Assimilation Scheme. *Quart. J. Roy. Meteor. Soc.,* **127,** 209–232.

Klemp, J. B., and R. B. Wilhelmson, 1978: Simulations of three-dimensional convective storm dynamics. *J. Atmos. Sci.,* **35,** 1070–1076.

Kuo, Y.-H., S. V. Sokolovsky, R. A. Anthes, and F. C. Vandenberghe, 2000: Assimilation of GPS radio occultation data for numerical weather prediction. *Terr. Atmos. Oceanic Sci.,* **11,** 157–186.

Liu, D. C., and J. Nocedal, 1989: On the limited memory BFGS method for large-scale optimization. *Math. Program.,* **45,** 503–528.

Lorenc, A. C., 1986: Analysis methods for numerical weather prediction. *Quart. J. Roy. Meteor. Soc.,* **112,** 1177–1194.

——, and Coauthors, 2000: The Met. Office global three-dimensional variational data assimilation scheme. *Quart. J. Roy. Meteor. Soc.,* **126,** 2991–3012.

Michalakes, J., S. Chen, J. Dudhia, L. Hart, J. Klemp, J. Middlecoff, and W. Skamarock, 2001: Development of a next-generation regional weather research and forecast model. *Developments in Teracomputing: Proceedings of the Ninth ECMWF Workshop*

on the Use of High Performance Computing in Meteorology, W. Zwiefnofer and N. Kreitz, Eds., World Scientific, 269–276.

Parrish, D. F., and J. C. Derber, 1992: The National Meteorological Center's Spectral Statistical Interpolation analysis system. *Mon. Wea. Rev.*, **120,** 1747–1763.

Purser, R. J., W.-S. Wu, D. F. Parrish, and N. M. Roberts, 2003a: Numerical aspects of the application of recursive filters to variational statistical analysis. Part I: Spatially homogeneous and isotropic Gaussian covariances. *Mon. Wea. Rev.*, **131,** 1524–1535.

——, ——, ——, and ——, 2003b: Numerical aspects of the application of recursive filters to variational statistical analysis. Part II: Spatially inhomogeneous and anisotropic general covariances. *Mon. Wea. Rev.*, **131,** 1536–1548.

Rabier, F., H. Järvinnen, E. Klinker, J.-F. Mahfouf, and A. Simmons, 2000: The ECMWF operational implementation of four-dimensional variational assimilation. I: Experimental results with simplified physics. *Quart. J. Roy. Meteor. Soc.*, **126,** 1143–1170.

Zou, X., F. Vandenberghe, M. Pondeca, and Y.-H. Kuo, 1997: Introduction to adjoint techniques and the MM5 adjoint modeling system. NCAR Tech. Note NCAR/TN-435 + STR, 110 pp. [Available from UCAR Communications, P.O. Box 3000, Boulder, CO, 80307.]